Supporting Information

1 Computational Methods

The frequency-dependent second-order nonlinear polarization P induced by an optical field can be expressed as:

$$P_a(2\omega) = \chi^{(2)}_{abc}(2\omega;\omega,\omega)\, E_b(\omega)\, E_c(\omega), \tag{1}$$

where $\chi^{(2)}_{abc}$ is the SHG susceptibility tensor (the superscript (2) denotes second-order nonlinearity), and a, b, c are Cartesian indices. $E_b(\omega)$ is the component of the incident electric field at frequency ω along direction b. We employ the *length-gauge* formalism for the calculation of SHG response, in which the total susceptibility $\chi^{(2)}_{abc}$ can be decomposed into three major contributions: the interband term $\chi^{\text{inter}}_{abc}$, the intraband term $\chi^{\text{intra}}_{abc}$, and the modulation term χ^{mod}_{abc}. Their relationship is given by

$$\chi^{(2)}_{abc}(2\omega;\omega,\omega) = \chi^{\text{inter}}_{abc}(2\omega;\omega,\omega) + \chi^{\text{intra}}_{abc}(2\omega;\omega,\omega) + \chi^{\text{mod}}_{abc}(2\omega;\omega,\omega). \tag{2}$$

Their explicit forms are as follows:

$$\chi^{\mathrm{inter}}_{abc}(2\omega;\omega,\omega) = \frac{e^3}{\hbar^2}\sum_{nml}\int_{\mathrm{BZ}}\frac{d\mathbf{k}}{4\pi^3}\frac{r^a_{nm}\{r^b_{ml}r^c_{ln}\}}{\omega_{ln}-\omega_{ml}}\left(\frac{2f_{nm}}{\omega_{mn}-2\omega}+\frac{f_{ml}}{\omega_{ml}-\omega}+\frac{f_{ln}}{\omega_{ln}-\omega}\right), \tag{3}$$

$$\begin{aligned}\chi^{\mathrm{intra}}_{abc}(2\omega;\omega,\omega) = \frac{e^3}{\hbar^2}\int_{\mathrm{BZ}}\frac{d\mathbf{k}}{4\pi^3}\Bigg[&\sum_{nml}\omega_{mn}r^a_{nm}\{r^b_{ml}r^c_{ln}\}\left(\frac{f_{nl}}{\omega^2_{ln}(\omega_{ln}-\omega)}-\frac{f_{lm}}{\omega^2_{ml}(\omega_{ml}-\omega)}\right)\\ &-8i\sum_{nm}\frac{f_{nm}r^a_{nm}\{\Delta^b_{mn}r^c_{mn}\}}{\omega^2_{mn}(\omega_{mn}-2\omega)}+2\sum_{nml}\frac{f_{nm}r^a_{nm}\{r^b_{ml}r^c_{ln}\}(\omega_{ml}-\omega_{ln})}{\omega^2_{mn}(\omega_{mn}-2\omega)}\Bigg],\end{aligned} \tag{4}$$

$$\begin{aligned}\chi^{\mathrm{mod}}_{abc}(2\omega;\omega,\omega) = \frac{e^3}{2\hbar^2}\int_{\mathrm{BZ}}\frac{d\mathbf{k}}{4\pi^3}\Bigg[&\sum_{nml}\frac{f_{nm}}{\omega^2_{mn}(\omega_{mn}-\omega)}\left(\omega_{nl}r^a_{lm}\{r^b_{mn}r^c_{nl}\}-\omega_{lm}r^a_{nl}\{r^b_{ml}r^c_{mn}\}\right)\\ &-i\sum_{nm}\frac{f_{nm}r^a_{nm}\{r^b_{mn}\Delta^c_{mn}\}}{\omega^2_{mn}(\omega_{mn}-\omega)}\Bigg].\end{aligned} \tag{5}$$

Here, $\omega_{nm}=\omega_n-\omega_m$ denotes the energy difference between bands n and m, while $f_{nm}=f_n-f_m$ represents the difference of their Fermi–Dirac occupation factors. $r_{nm}=v_{nm}/(i\omega_{nm})$ is the position-operator matrix element, and $\{r^b_{ml}r^c_{ln}\}=\frac{1}{2}(r^b_{ml}r^c_{ln}+r^c_{ml}r^b_{ln})$ is the symmetrized product. $\Delta^b_{mn}=v^b_{mm}-v^b_{nn}$ corresponds to the difference in the diagonal velocity matrix elements along the b direction. In the practical calculation, a small phenomenological broadening factor δ is introduced as $\omega\to\omega+i\delta$ with $\delta=0.1\,\mathrm{eV}$, in order to avoid divergences when the photon energy coincides with band transition resonances.

2 Band Structure With Concentration of Defects

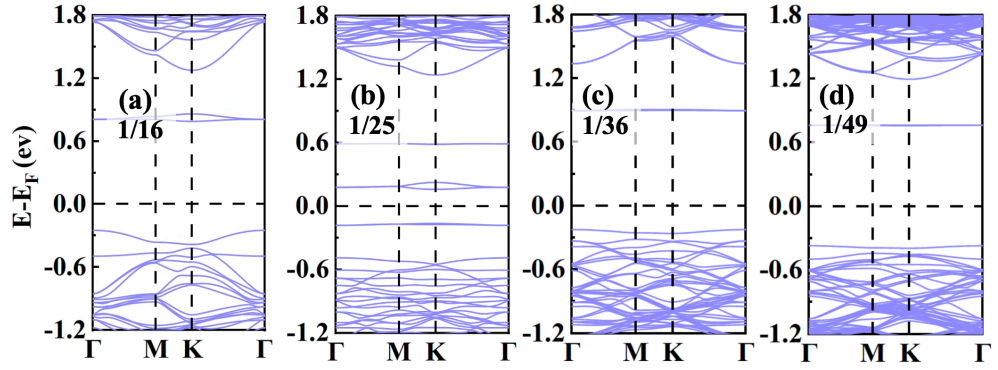

Figure 1: Band structures of the V_S defect type at different defect concentrations. (a) Band structure at 1/16 concentration. (b) Band structure at 1/25 concentration. (c) Band structure at 1/36 concentration. (d) Band structure at 1/49 concentration.

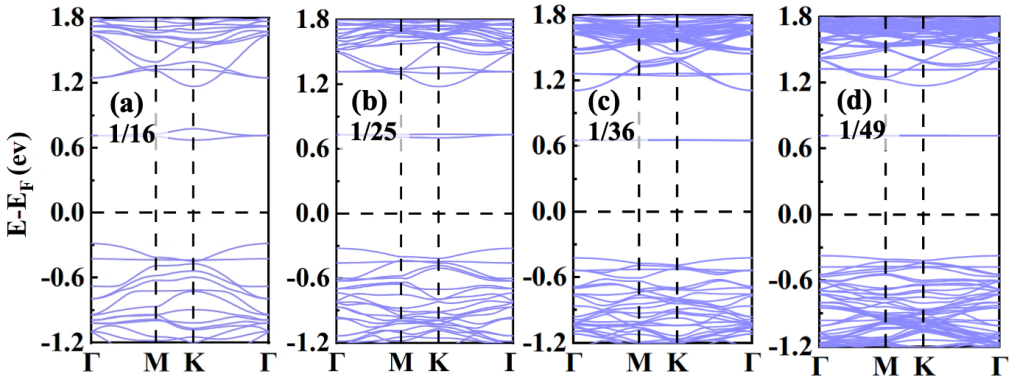

Figure 2: Band structures of the V_{S2} defect type at different defect concentrations. (a) Band structure at 1/16 concentration. (b) Band structure at 1/25 concentration. (c) Band structure at 1/36 concentration. (d) Band structure at 1/49 concentration.

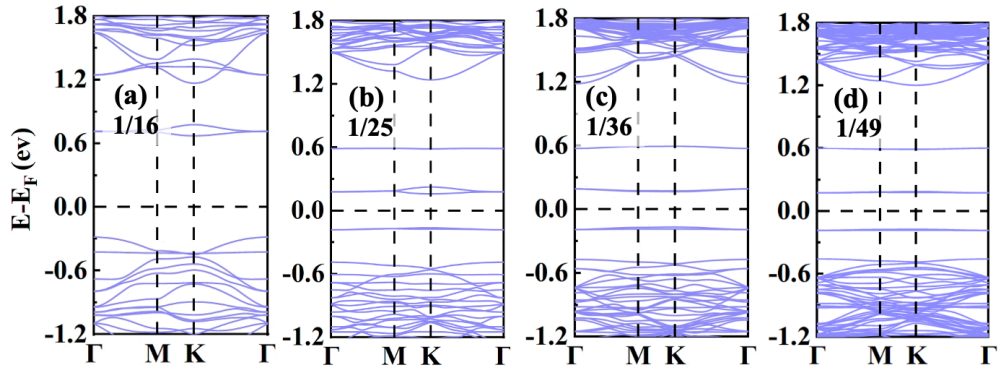

Figure 3: Band structures of the V_{Mo} defect type at different defect concentrations. (a) Band structure at 1/16 concentration. (b) Band structure at 1/25 concentration. (c) Band structure at 1/36 concentration. (d) Band structure at 1/49 concentration.

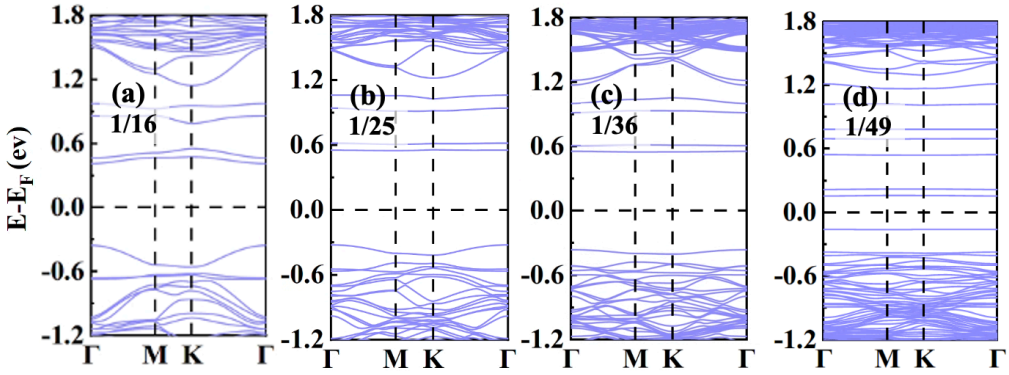

Figure 4: Band structures of the $V2_{S2}$ defect type at different defect concentrations. (a) Band structure at 1/16 concentration. (b) Band structure at 1/25 concentration. (c) Band structure at 1/36 concentration. (d) Band structure at 1/49 concentration.

3 SHG variation with defect concentration

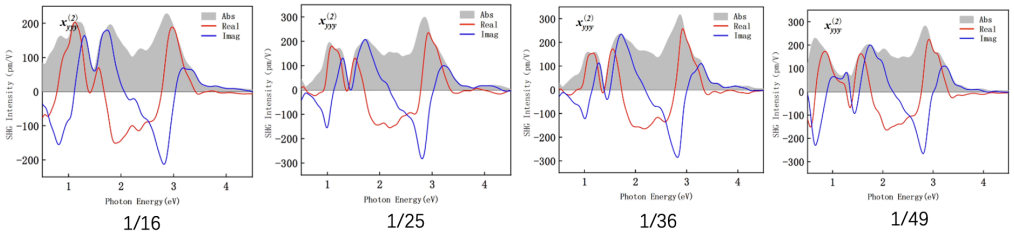

Figure 5: SHG response of the $V2_{S2}$ defect type at different defect concentrations.

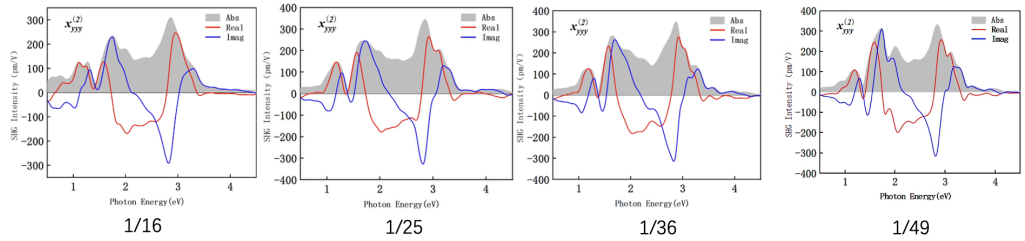

Figure 6: SHG response of the V_S defect type at different defect concentrations.

4 All SHG components with different defect types in 4X4 supercell

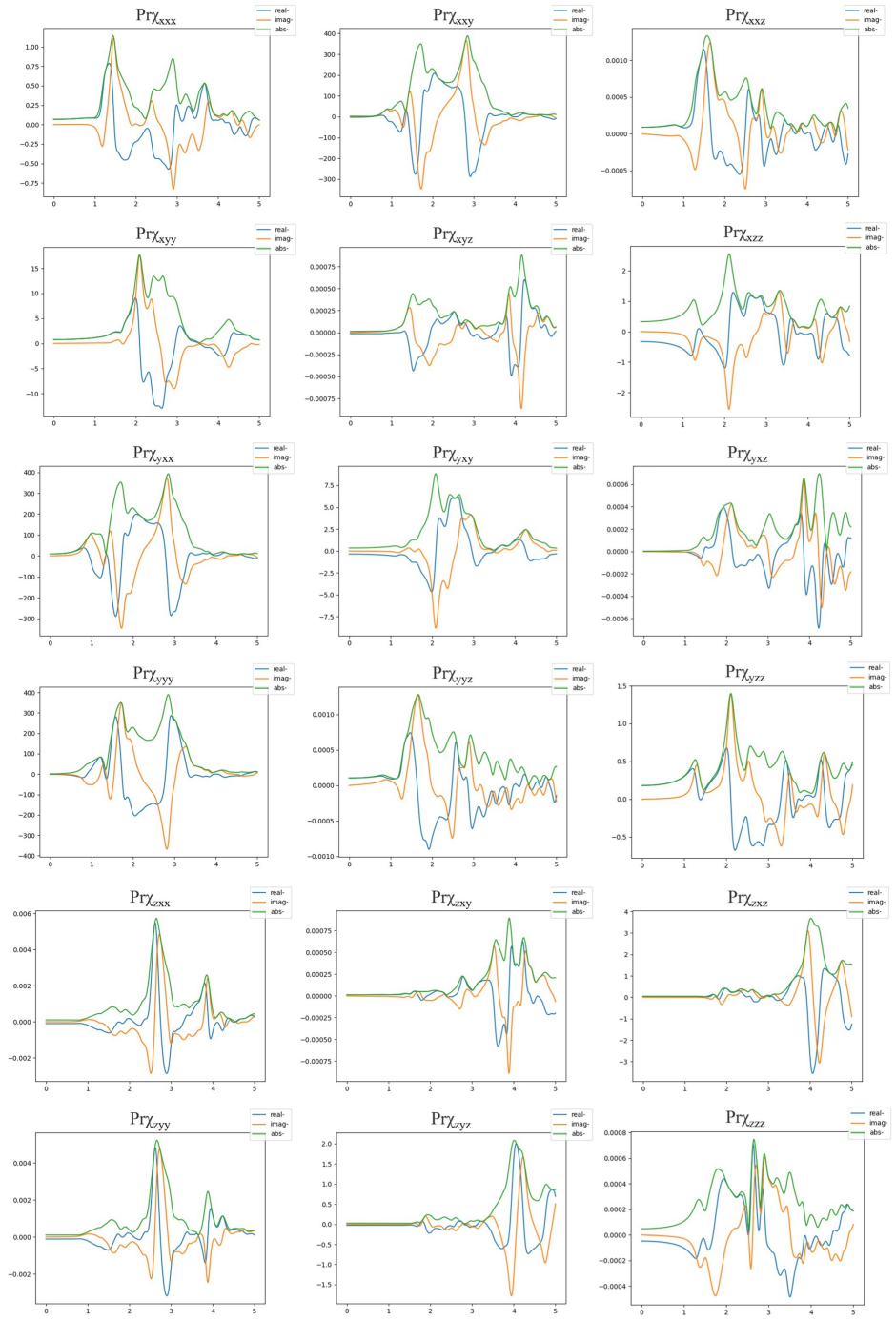

Figure 7: All SHG components with pristine MoS_2 in 4X4 supercell

Figure 8: All SHG components with Mo_S with defects in 4X4 supercell

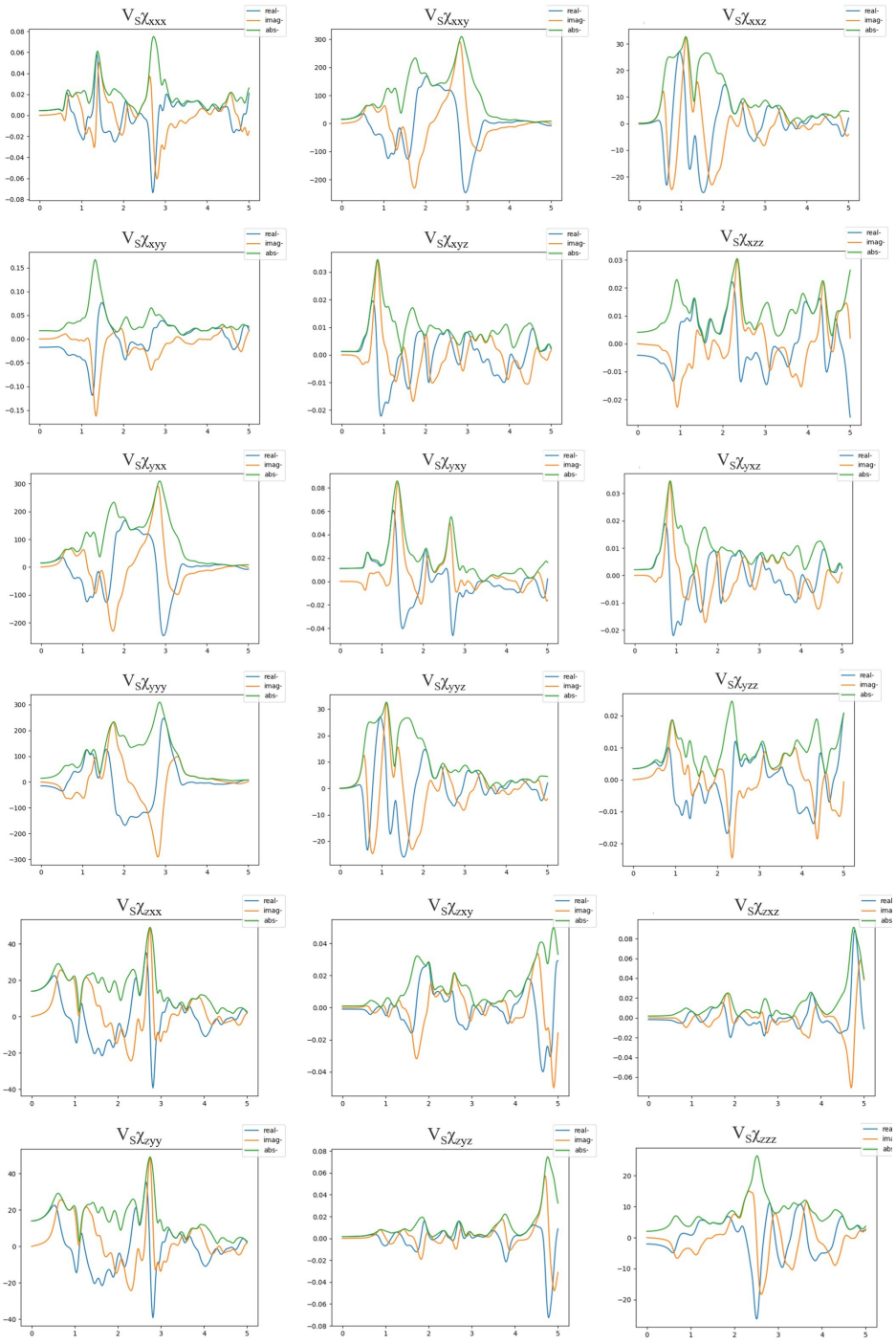

Figure 9: All SHG components with V_S with defects in 4X4 supercell

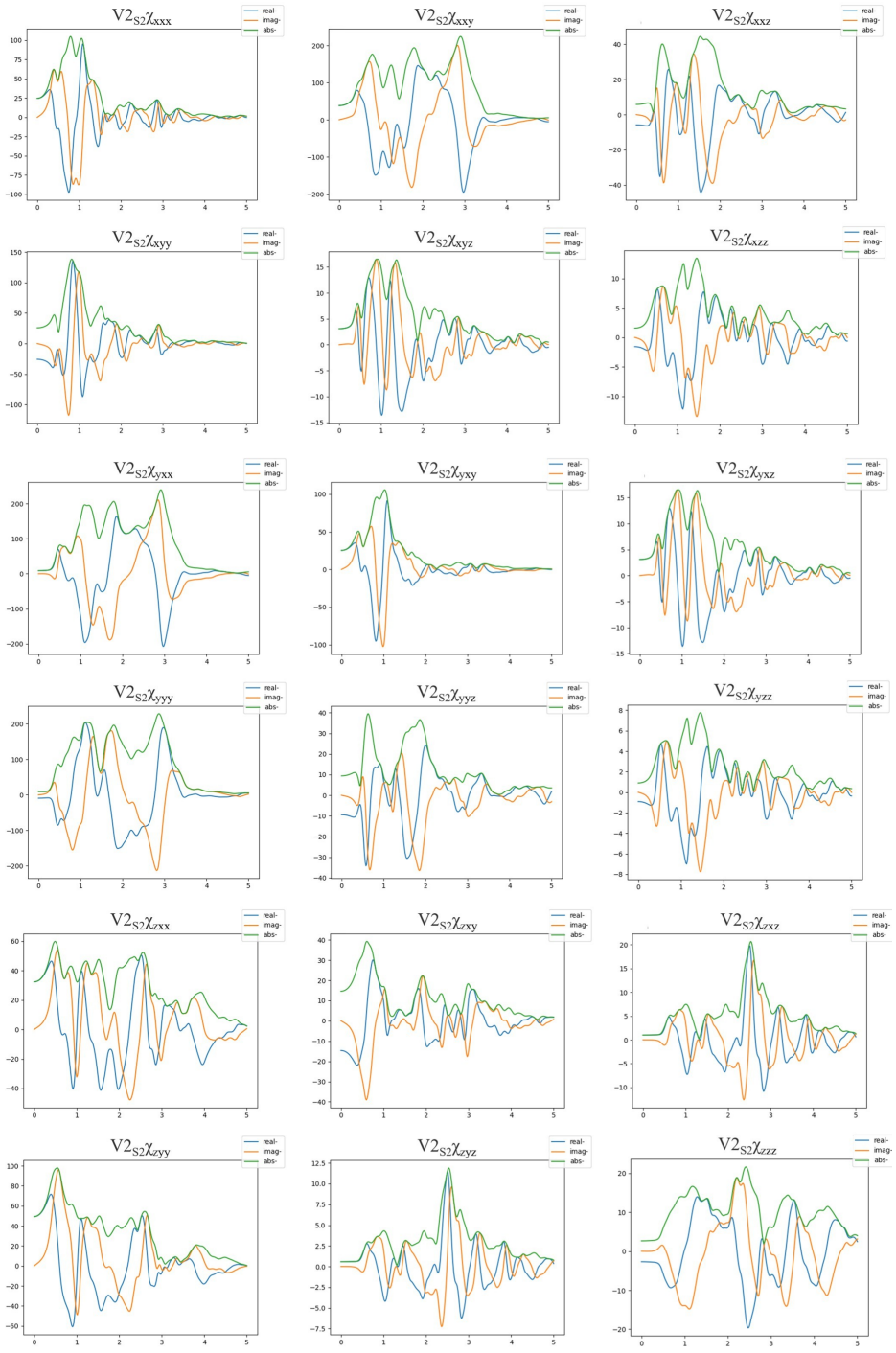

Figure 10: All SHG components with $V2_{S2}$ with defects in 4X4 supercell

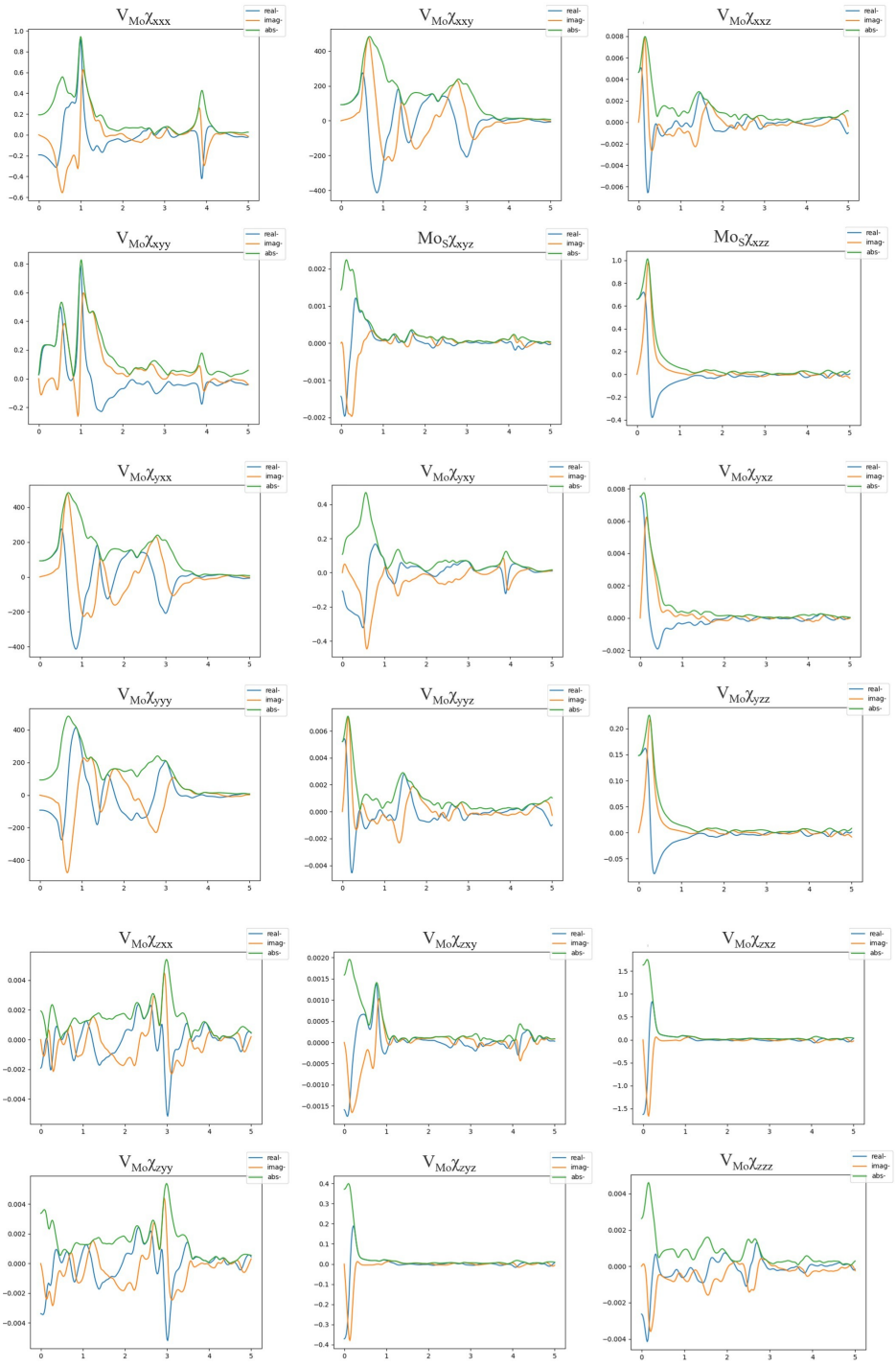

Figure 11: All SHG components with V_{Mo} with defects in 4X4 supercell